CHARACTERIZING MOLECULAR HETEROGENEITY OF STEM CELL EPIDERMAL LINEAGES

A Thesis

Presented to the Faculty of the Graduate School

of Cornell University

In Partial Fulfillment of the Requirements for the Degree of

Master of Science

by

Tara Elizabeth Hall

May 2019

ABSTRACT

Recent studies in the Tumbar Laboratory have identified heterogenous domains in the interfollicular epidermis of skin based on gene expression patterns. These heterogenous domains are inhabited by two types of stem cells; slow cycling label retaining cells (LRCs) and fast cycling non-LRCs. My work has focused on identifying genetic markers for the slow cycling LRCs. I critically investigated previous microarray data obtained from LRCs and nonLRC analysis to identify genes that were preferentially expressed in LRC domains. Two new potential markers of epidermal LRCs have been identified, however, based on immunofluorescent studies, these two genes were not found to overlap with the strongest LRCs. Instead they overlapped with LRCs that had partially reduced label. These gene expression domains are also spatiotemporally dynamic. Therefore, these midrange LRCs may indicate a third epidermal stem cell population. This opens the way to further functional studies to elucidate the role of gene expression heterogeneity in the epidermis.

BIOGRAPHICAL SKETCH

Tara Elizabeth Hall returned to school full-time in 2013 after serving in the US Army for nine years and working as a civilian instructor at US Army Intelligence schools for four years. While her military experience was not related to biology, her love of science and genetics prompted her to pursue her education in Molecular and Cellular Biology at the University of Arizona. In 2015 she received her Bachelor of Science and made the decision to continue her education by applying to graduate school. She was accepted to and began attending the Biomedical and Biological Sciences program at Cornell in 2016, where she received a SUNY Graduate Diversity Fellowship. Her interest in studying stem cells was prompted by several of the injuries she saw fellow soldiers suffer from. She was inspired learn and research stem cell function by the hope that better understanding will lead to advances in healing traumatic injuries.

ACKNOWLEDGMENTS

As mentor, Dr. Tudorita Tumbar provided the initial research goal and support and evaluation during the course of my research. My colleagues in the lab, Dr. Prachi Jain, Dr. Sangeeta Ghuwalewala and fellow graduate student Sangjo Kang lent me their expertise and help as well as samples. Funding was provided by the SUNY Graduate Diversity Fellowship and the NIH.

TABLE OF CONTENTS

CHAPTER 1

Introduction

The skin is an excellent organ, constantly renewing itself throughout an animal's life. This renewal is due to stem cells located within the basal layer of the epidermis. As part of the Tumbar Lab, my research has been on characterizing gene expression in stem cells within the epidermis, the outer most layer of the skin. Recent studies in our laboratory have identified heterogenous domains of gene expression in the skin interfollicular epidermis (Sada A et al, 2016). These heterogenous domains are inhabited by two types of stem cells; slow cycling label retaining cells (LRCs) and fast cycling non-LRCs. My work has focused on identifying genetic markers for slow cycling LRCs. Previously, two genes Slc1a3 and Dlx1, were identified as being preferentially expressed by either basal LRCs or non-LRCs respectively. However, Dlx1 was not detectable at the protein level and the Dlx1-CreER genetic driver marks only rare LRCs within the epidermis. Therefore, I revisited the previous microarray data to investigate genes that were preferentially expressed in LRCs to identify better candidates to serve as markers and for functional studies. By identifying genes expressed at higher levels (2x or more) in LRC basal and suprabasal populations over non-LRC populations in microarray data, we will be able to use these genes as markers for stem cells through immunofluorescent (IF) imaging, revealing heterogeneous domains that correspond to regions populated with LRCs. Studying genetic markers can reveal pieces to the puzzle of how stem cells operate, e.g. studying knock out lines. While identifying stem cell markers for mouse skin is a useful tool, a portion of my goal has been to also identify markers of stem cells in human skin. To that end, collaboration with other laboratories has provided us with human skin samples.

Through my studies in the Tumbar Laboratory, I have identified two new potential markers of epidermal LRCs: Arfgap3 and Vamp1. Arfgap3 is a GTP-ase activating protein, regulating the early secretory pathway of proteins by associating with the Golgi apparatus (Arfgap3, 2019). This protein promotes the hydrolysis of ADP-ribosylation factor 1 (ARF1)-bound GTP, which is required for the dissociation of coat proteins from Golgi-derived membranes and vesicles. Dissociation of the coat proteins is a prerequisite for the fusion of these vesicles with target compartments (Arfgap3, 2019). Within the cell, it is expressed strongly in the cytosol, Golgi apparatus, and moderately in the nucleus (ARFGAP3 localizations, 2019). Vamp1 is a vesicle associated membrane protein, part of a complex that is involved with the docking and fusion of synaptic vesicles (Vamp1, 2019). Vamp1 is involved in the targeting and fusion of transport vesicles to their target membrane and docking of vesicles at the pre-synaptic membrane. It is found along cell membranes in association with formation of vesicles (Salpietro, 2017) see also Table 1. Within the cell, it is strongly expressed in the plasma membrane, the cytosol, and mitochondria (VAMP1 localizations, 2019).

I found that Arfgap3 and Vamp1 are expressed in heterogenous domains but not with the slowest cycling stem cells which retain the most label. Instead, these genes are expressed by LRCs which have divided but not enough to completely lose the label. The heterogenous domains also do not completely align with midrange LRCs but can include cells immediately adjacent. Further functional studies utilizing knock-out mouse model lines could elucidate the role of Vamp1 and Arfgap3 gene expression heterogeneity in the epidermis.

Gene symbol Full Gene name	BL fold change SL fold change	Gene function	Antibodies	Transgenic lines	References
Abca5, ATP-binding cassette, sub-family A, member 5	10.5204 2.2005	Carries molecules across extra and intracellular membranes.	Abcam rb polyclonal cat.no. ab99953	Osaka University; Kubo Y, et al. 2005. EuMMCR; Abca5tm1a(EUCOMM)Wtsi, ES cells.	DeStefano GM, et al. 2014. Hayashi R, et al. 2017.
Arfgap3*, ADP Ribosylation Factor GTPase Activating Protein 3	7.7397 3.965	Associates with Golgi apparatus, regulates the early secretory pathway of proteins. Promotes the dissociation of coat proteins from Golgi-derived membranes and vesicles.	Novus Biological rb poly cat.no. NBPI-88842/NBPI-31064; Abcam rb mono cat.no. ab183746; GeneTex rb poly cat.no. GTX87479/GTX55515; **Proteintech rb poly cat.no. 15293-1-AP**	Requires custom ordering; all previous research conducted with transfected cells only	Dembla M, et al. 2014. Tšuiko O, et al. 2016.
Arhgef28 (aka Rgnef)*, Rho Guanine Nucleotide Exchange Factor	6.7184 7.2951	Interacts with low molecular weight neurofilament mRNA. Functions in axonal branching, synapse formation and dendritic morphogenesis, focal adhesion formation, cell motility.	BD Biosciences m mono cat.no. 610149; Novus Biologicals gt poly cat.no. NBP2-42484; MediMabs gt poly cat.no. MM-0193-P-50; Antibodies Online gt poly cat no. ABIN2443867/ ABIN2443868	UC San Diego; Miller NL, et al. 2012. Moores UCSD Cancer Center; Miller NL, et al. 2013.	Nakahara H, et al. 1998. Lim Y, et al. 2008. Lim ST, et al. 2010.
Cacul1 , CDK2 associated, cullin domain 1	5.1767 2.058	Cell cycle associated protein capable of promoting cell proliferation through the activation of CDK2 at the G1/S phase transition.	Abcam rb mono cat.no. ab190799	MMRRC; ES cells knock out, 007912-UCD-CELL, line XF165.	Kigoshi Y, et al. 2015.
Etfdh*, Electron Transfer Flavoprotein Dehydrogenase	5.1221 7.9579	Component of electron-transfer system in mitochondria, essential for electron transfer from mitochondrial flavin-containing dehydrogenases to main respiratory chain.	Abcam m mono cat.no. ab131376; Santa Cruz Biotechnology m mono cat.no. sc-515202	Shandong University; Xu J, et al. 2018 (knock in line).	Roselló-Lletí E, et al. 2014.
Nagk*, N-Acetyl glucosamine Kinase	9.0603 3.6032	Converts endogenous GlcNAc from lysosomal degradation/ nutritional sources to GlcNAc 6-phosphate. Related pathways include metabolism of proteins, transport to the Golgi, subsequent modification.	Sigma Aldrich ck poly cat.no. GW22347; Novus Biologicals rb poly cat.no. NBP1-89750; Antibodies Online rb poly cat.no. ABIN872749; **Proteintech rb poly cat.no. 15051-1-AP**	MMRRC; 011739-UCD-EMBRYO, 011739-UCD-RESUS, 011739-UCD SPERM	Sharif SR, et al. 2016.
Rapgef4 (aka Epac, Epac2), Rap guanine nucleotide exchange factor	11.6079 4.534	Guanine nucleotide exchange factor for Ras-like small GTPase Rap upon cAMP stimulation. Involved in a variety of cAMP-mediated cellular functions in endocrine and neuroendocrine cells and neurons.	Abcam rb poly cat no. ab124189/ ab21238; Santa Cruz Biotechnology m mono cat no. sc-28326; **Proteintech rb poly cat.no. 19103-1-AP**	Kyungpook National University; Seo H, Lee K, 2016. UC Davis; Pereira L, et al. 2013. Jax Labs, stock #018390. Kobe University; Zhang CL, et al. 2009.	Wallner M, et al. 2015. Masyuk AI, et al. 2008.
Rpap2 , RNA polymerase II associated protein 2	5.8098 4.306	Protein phosphatase, displays CTD phosphatase activity, regulates transcription of snRNA genes. Mainly cytoplasmic protein that shuttles between the cytoplasm and the nucleus.	**Proteintech rb poly cat.no.** 17401-1-AP/ **17401010AP**; Thermo Fisher Scientific rb poly (human reactive) cat.no. PA5-61244; Novus Biologicals rb poly (human reactive) cat.no. NBP2-13248	IMPC: KOMP, ES cell available	Guglielmi V, et al. 2015. Forget D, et al. 2013.
Vamp1, Vesicle associated membrane protein 1	21.1402 9.9531	Involved in the docking and/or fusion of synaptic vesicles with presynaptic membrane, in the targeting and/or fusion of transport vesicles to their target membrane.	Abcam rb poly cat.no. Ab3346; **Proteintech rb poly cat.no.13115-1-AP**	Jax Labs, stock #004626. EUCOMM, HEPD0509.	Corderiro JM, et al. 2013. Morgenthaler FD, et al. 2003. Nystuen AM, et al. 2007. Peng L, et al. 2014. Riffault B, et al. 2014. Tsai PS, et al. 2011. Rossetto O, et al. 1996. Duregotti E, et al. 2015.

Table 1 Potential LRC markers. Genes were initially selected based on fold change values. Genes with published research and validated antibodies were then selected. Genes marked with * were passed over at first due to lack of publications with desired antibodies or lack of research overall. The antibodies listed were found on supplier's websites. These genes were included in qRT-PCR analysis in order to have a starting group size of around 10 candidates. Antibodies in bold were used in immunofluorescent analysis.

CHAPTER 2

Results

A. Identifying LRC marker candidates based on microarray data mining.

Previously the Tumbar laboratory has generated gene expression profiles by microarrays of sorted LRC and non-LRC cell populations isolated from the basal and suprabasal layers of the adult mouse epidermis. Skin cells were sorted into epidermal LRCs with progeny, non-LRCs with progeny, and the uppermost layer of living cells regardless of origin. These were subjected to microarray analysis. Sorting criteria removed any stem cells found in the hair follicle (Sada A et al, 2016). Previous comparisons of microarray data focused on identifying markers uniquely upregulated in the basal layer LRCs relative to all other sorted populations for lineage tracing purposes (Sada A et al, 2016). We reasoned that this approach might have left out a number of genes expressed differentially between LRC versus nonLRC epidermal domains that span both basal and suprabasal layers. To verify this, I compared and sorted gene expression microarray values between groups of all epidermal cell populations namely basal layer (BL) LRCs and non-LRCs, spinous layer (SL) LRCs and non-LRCs, and granular layer (GL). I did this in a step-wise algorithm comparing populations two by two to yield probe sets that were expressed two-fold higher in both basal and suprabasal LRCs relative to all nonLRCs, whereas the granular layer expression was un-restricted. This comparison resulted in a group of 210 probe sets with a distinctive expression pattern when visualized in a heatmap (Fig 1a). The pattern demonstrates the desired result of the compared sorting scheme, with genes up-regulated in LRC basal and spinous layers and down-regulated in non-LRC basal and spinous layers. The genes with the highest fold change difference between epidermal LRCs and nonLRCs, which were also judged as good candidates for

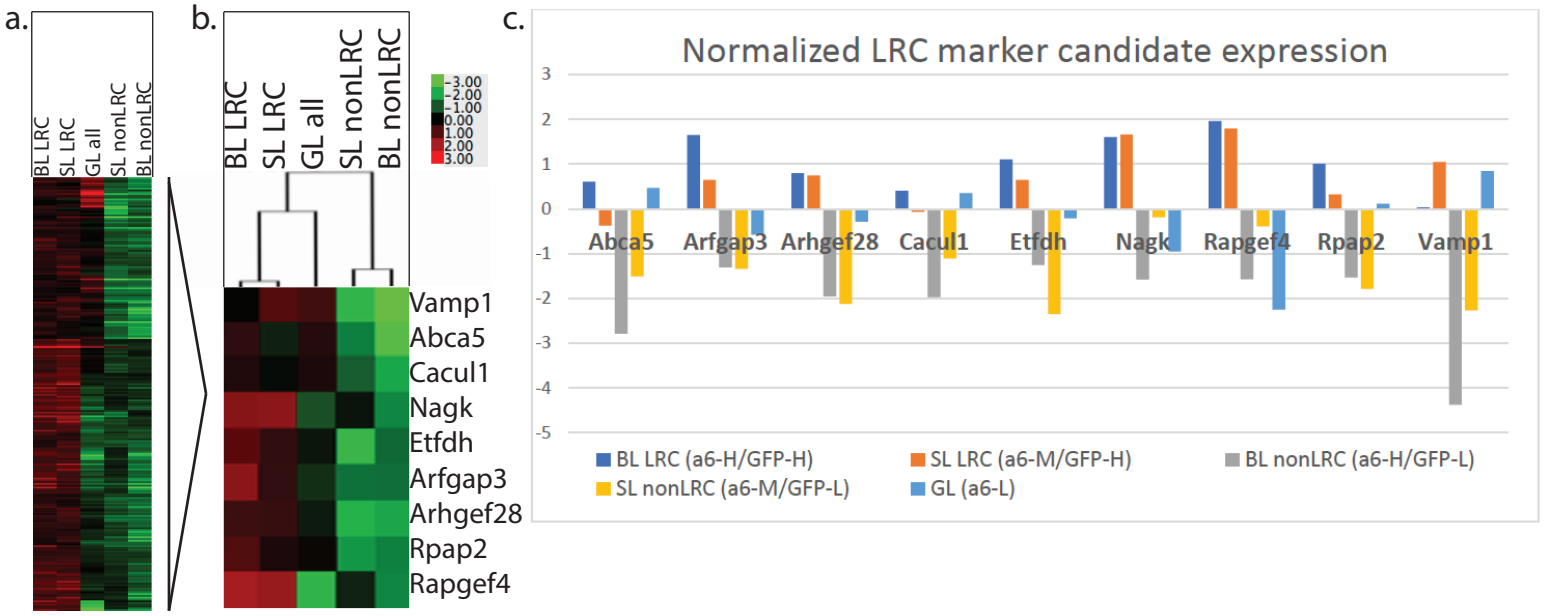

Figure 1 Analysis of microarray data and gene selection criteria. a. Heatmap of 210 genes sorted for preferential expression in LRCs over non-LRCs. Legend of relative expression levels. b. Genes selected for analysis. c. Graph of gene relative expression of genes selected for analysis. Vamp1 had relatively low BL LRC expression but had largest overall difference between LRC and nonLRC populations. A vendor was identified which carried a 20µl sample aliquot of Vamp1, making it a low-cost option to examine protein expression through IF. Arfgap3, Nagk, Rapgef4, and Rpap2 are upregulated in both LRC populations and were available as sample aliquots also so were included in the IF examination of protein expression.

future functional studies based on my literature searches, were selected for further analysis (Fig 1b, Table1). Their actual fold changes in the different sorted epidermal populations are shown in Fig 1c.

To verify that these gene candidates are indeed expressed in the skin I isolated RNA from adult mouse skin and tested its quality on a gel followed by cDNA synthesis through reverse transcriptase (data not shown). I then designed primers to all 10 candidates that would be suitable for quantitative reverse-transcriptase qRT-PCR using to capture all isoforms of the genes, and wherever possible to span introns to eliminate any potential genomic DNA contamination (Table 2). I measured gene expression in whole skin and sorted cells via qRT-PCR (Fig 2). The CT values obtained in this experiment were high but dependent on input concentration (1 ng and 10ng RNA/reaction), suggesting low but detectable levels of expression of our gene candidates in the skin. Since LRCs make up a relatively low portion of the whole skin cell populations, the expression of these gene candidates is expected to be low in whole skin isolates.

I repeated the RNA isolation, cDNA synthesis and qRT-PCR analysis using RNA isolated from sorted cells Fig 2d, e). Since cDNA from epidermal LRCs and non-LRCs were no longer available in the laboratory, I tested available cDNAs from bulge (CD34+/a6-integrin+) and non-bulge (CD34-/a6-integrin+) cells previously sorted in our laboratory. The paucity of RNA constrained the qRT-PCR analysis to 0.1ng of cDNA per well, and the CT values are relatively high but still indicate detectable gene expression. This encouraged me to pursue study of these gene further, and I was able to move on to IF studies to visualize their protein expression in the epidermis.

Gene name	primer direction	Primer sequence
Vamp1	Forward	AGAGTTCCGGGTGTTTCGTG
Vamp1	Reverse	CCGCCTGTTACTGGTCATGT
Nagk	Forward	GCACAAACCACTGGCTGATT
Nagk	Reverse	CGGTGCCTCAACTCCTCAAT
LIF	Forward	GGCAACCTCATGAACCAGATC
LIF	Reverse	TCTGGTCCCGGGTGATATTG
Cacul1	Forward	AACACCTCCACCTCCAAGTT
Cacul1	Reverse	CTGCTGGCACACACACTTAT
Arfgap3	Forward	TCTAGCTGGGATGATGGTGC
Arfgap3	Reverse	TGAAGAGATGGCCTTGACGT
Etfdh	Forward	TGAGCTGGATGGGAGAACAG
Etfdh	Reverse	ACTTTGGCATGCAGTTCCAG
Arhgef28	Forward	AGTCTTGGAGTCTCGTGGTG
Arhgef28	Reverse	AGCTGCAGTTCCTCCTTCAT

Table 2 Primers designed for qRT-PCR analysis of candidate gene expression in whole skin and sorted cell analysis.

Experiment 1

a.

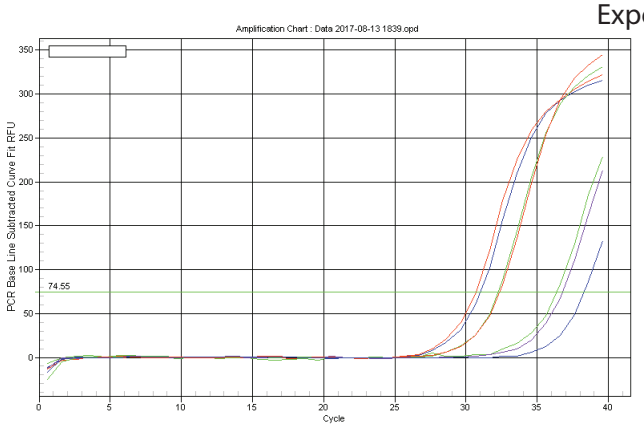

b.

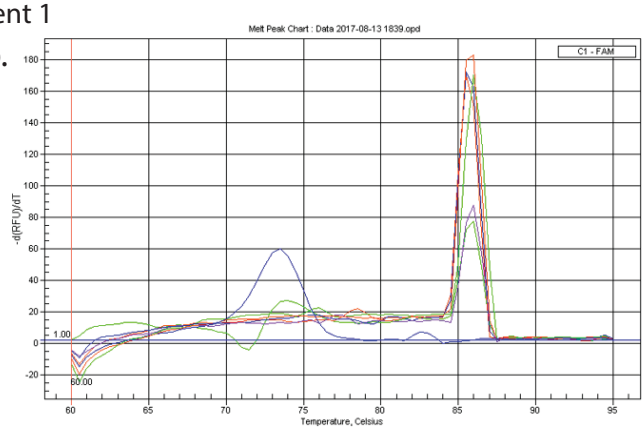

c.

		Vamp1	Abca5	Nagk	Etfdh	Arfgap3	Arhgef28	Cacul1	Rpap2	Rapgef4	LIF	Gapdh
F166 M6 whole skin	1ng ThresholdCycle	36.34	29.58	29.83	29.90	30.82	30.37	28.70	31.71	31.74	31.11	23.31
	10ng ThresholdCycle	30.71	25.90	26.03	26.12	26.82	26.92	25.15	28.21	29.91	29.38	19.42
	10ng ThresholdCycle	31.00	25.78	25.94	26.20	26.51	27.05	25.36	27.50	29.90	29.30	19.55
F165 M2 whole skin	1ng ThresholdCycle	36.76	29.99	30.69	30.94	31.65	31.59	29.62	31.79	32.94	29.20	24.12
	10ng ThresholdCycle	32.26	27.14	27.89	27.37	28.44	28.35	26.50	29.72	31.30	29.10	20.93
	10ng ThresholdCycle	32.38	27.26	27.79	27.37	28.47	28.75	26.73	29.48	30.73	29.66	20.87
H_2O	0ng ThresholdCycle	38.28	35.84	31.52	34.70	34.12	32.95	35.26	31.96	32.81	29.69	30.54

Experiment 2

d.

		Vamp1	Abac5	Nagk	Etfdh	Arfgap3	Arhgef28	Cacul1	Rpap2	Rapgef4	Gapdh
Sorted, bulge	Bulge	M1	M1	M1	M1	M1	M2	M2	M2	M2	M2
	ThresholdCycle	36.61	33.43	32.82	34.11	33.02	32.25	34.95	N/A	N/A	28.82
	Bulge	M3	M3	M3	M3	M3	M4	M4	M4	M4	M4
	ThresholdCycle	33.10	29.61	29.69	28.79	29.50	28.94	30.30	31.47	34.35	25.62
Sorted, non-bulge	non Bulge	M1	M1	M1	M1	M1	M2	M2	M2	M2	M2
	ThresholdCycle	31.69	29.70	29.10	27.99	28.83	27.47	28.60	31.16	30.15	23.25
	non Bulge	M3	M3	M3	M3	M3	M4	M4	M4	M4	M4
	ThresholdCycle	34.01	31.65	31.03	31.31	N/A	35.14	33.20	34.73	N/A	28.99

Experiment 3

e.

		Vamp1	Abca5	Nagk	Etfdh	Arfgap3	Arhgef28	Cacul1	Rpap2	Rapgef4	Gapdh
Sorted, non-bulge cells 0.1ng	M3D1 ThresholdCycle	32.96	31.74	30.90	31.78	30.61	N/A	29.67	32.22	31.63	26.21
	M3D1 ThresholdCycle	33.76	31.48	27.43	30.91	31.29	N/A	30.05	34.73	31.59	25.88
	M3D3 ThresholdCycle	N/A	30.94	28.96	29.50	30.31	N/A	28.41	30.59	30.24	24.36
	M3D3 ThresholdCycle	31.75	30.92	29.04	29.28	30.49	N/A	29.03	31.86	29.77	24.68
	M4 ThresholdCycle	N/A	N/A	30.99	31.51	30.72	N/A	30.78	33.68	32.61	26.93
	M4 ThresholdCycle	N/A	32.02	31.19	31.14	30.60	N/A	30.13	N/A	30.88	26.83
H_2O	0ng ThresholdCycle	N/A	N/A	31.85	N/A	31.73	N/A	N/A	N/A	34.69	36.05

Figure 2 qRT-PCR analysis of gene expression in whole skin and sorted cell samples. a. Vamp1 qPCR amplification curve showing 0, 1, and 10ng samples. b. Vamp1 qPCR melt peaks of 0, 1, and 10ng samples. c. All tested primers qPCR CT values at 0, 1, and 10ng. d. All tested primers (excepting LIF) qPCR CT values at 0.1ng in sorted cell samples. Samples were sorted into bulge and non-bulge (CD34- and alpha6+) populations. e. All tested primers (excepting LIF) qPCR values at 0.1ng in sorted cell samples. Samples were non-bulge (CD34- and alpha6+) cells.

B. Testing patterns of LRC marker candidate expression by skin immunofluorescence studies.

In order to visualize the protein expression in the epidermis of my epidermal LRC candidates I performed immunofluorescence studies in parallel with the qPCR studies described above. I purchased antibodies for 5 of my 10 candidate genes described above (Table 3) and stained skin sections at different stages and with different dilutions of my primary antibodies. Three of my tested candidates (Nagk, Rpap2, Rapgef4) did not show reliable signal nor discernable heterogenous expression patterns within the epidermis and their evaluation was discontinued. In contrast, two candidates (Vamp1 and Arfgap3) indicated heterogenous expression within the epidermal layer and prompted us to examine their expression at different time points, with different markers of differentiation and with transgenic skin samples, using a tet-repressible Keratin5-driven H2B-GFP pulse chase to mark LRCs. Below I will describe in more details the results of these immunofluorescence experiments.

B1. Vamp1 and Arfgap3 are expressed in distinct domains in mouse back skin.

To understand Vamp1 and Arfgap3 protein expression pattern in the skin and examine potential heterogeneity in the epidermis I stained back skin sections with a Vamp1 or Arfgap3 antibody. Mice were sacrificed at different time points during adult skin homeostasis including postnatal day (PD) 28, PD39, PD49 PD56, and skin tissue was embedded in OCT, sectioned, and stained with antibodies to either Vamp1 or Arfgap3. Various markers of differentiation such as α6-integrin and Keratin 14 (K14) for basal layer and Keratin 10 (K10) for spinous layer were used as counterstain (Fig 3, 4).

Gene	Supplier	Cat. No	Source	Isotype	Dilution
Arfgap3	Proteintech	15293-1-AP	Rabbit	IgG	**1:500,** 1:300, 1:250, 1:200, 1:150, 1:100, 1:50
Epac2 (Rapgef4)	Proteintech	19103-1-AP	Rabbit	IgG	1:400, 1:300, 1:200, 1:100
Nagk	Proteintech	15051-1-AP	Rabbit	IgG	1:500, 1:250, 1:100
Rpap2	Proteintech	17401010AP	Rabbit	IgG	1:500, 1:250
Vamp1	Proteintech	13115-1-AP	Rabbit	IgG	1:800, **1:500,** 1:300, 1:400, 1:200, 1:100

Table 3 Antibodies used in immunofluorescent analysis. All dilutions tested are listed. Effective dilutions in bold.

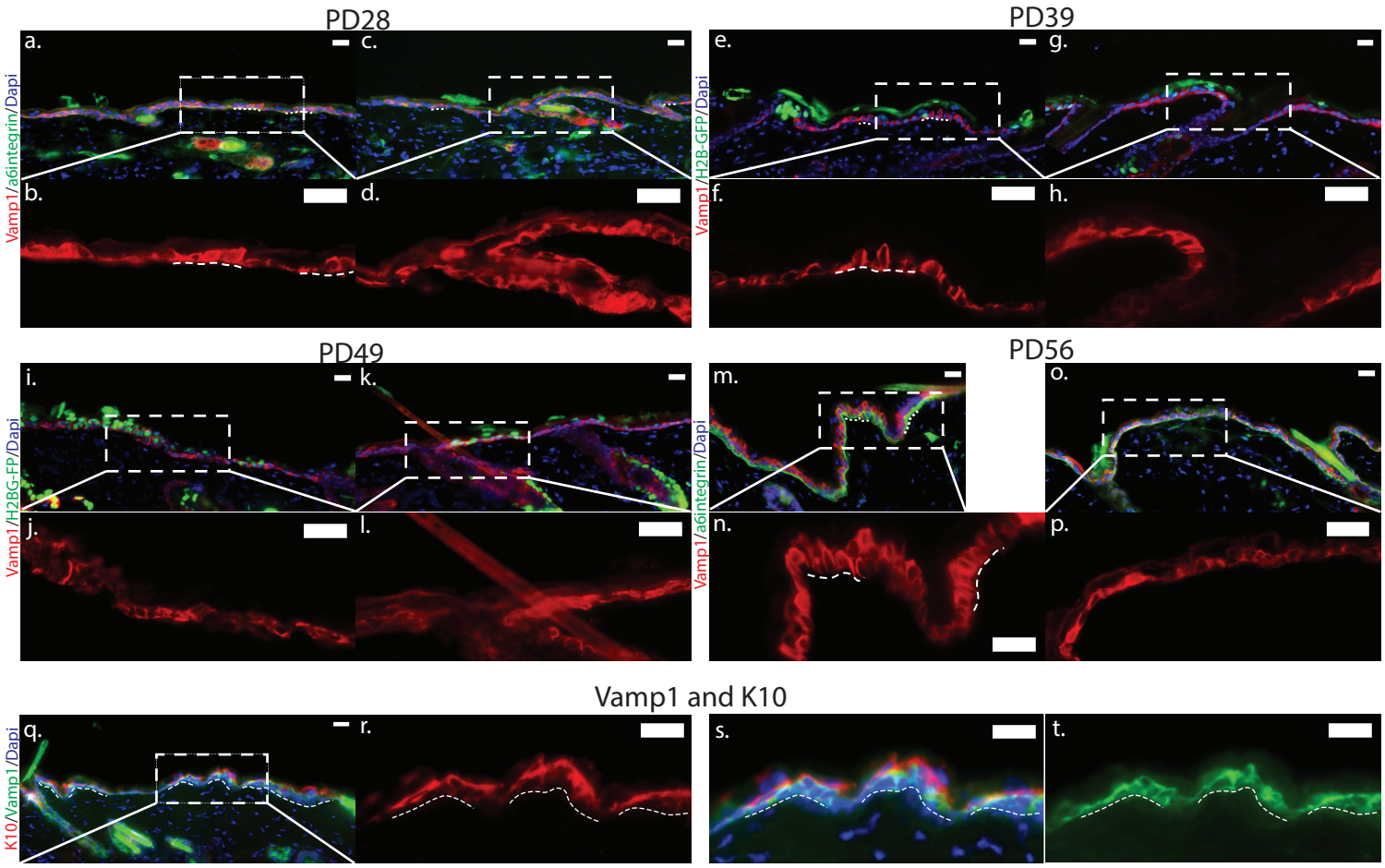

Figure 3 Vamp1 expression in mouse back skin at varying time points.

a-d PD28: a. Heterogeneity is greatest, with smaller domains. In the interfollicular epidermis, expression is much choppier at this stage, with levels of expression alternating with cells, or with high expressing cells in small groups of two to three. The cell shape is clearly outlined by the Vamp1 expression. Low expressing cells show Vamp1 at the basal membrane contacting side. c. Near the infundibulum, there tends to be a larger, consistently high expressing group of cells. This group of cells is linear, continuing to show basal expression (d), and covers the epidermis near the infundibulum and continues just into the beginning of it. Cells that express Vamp1 highly have a higher profile than other cells (dashed lines).

e-h PD39: e. High expressing cells show Vamp1 covering a continuous region. f. Domain size increases with stronger expression in vicinity of hair follicles and this trend continues in PD49-56. Low expressing cells show Vamp1, though noticeably less than the high expressing cells. There are small regions where it appears cells do not express Vamp1. Regions of high Vamp1 expression include the epidermis proximal to the infundibulum (f, g). Cells expressing Vamp1 highly often take on a tall narrow shape with a wider base than tip, much like a flame (f).

i-l PD49: i. Expression is broad, with smaller regions of no expression. Vamp1 is expressed at higher levels throughout the basal layer. Most of the IFE basal layer expresses Vamp1 (i), though Vamp1 expression next to the infundibulum appears to be stronger (k). In contrast to PD 28 and 39, cells expressing Vamp1 at higher levels do not have a higher profile or flame shape but share the shapes of cells that do not express Vamp1 being globular (j) or even flattened (l).

m-p PD56: m. Vamp1 is strongly expressed in the majority of the basal layer. There are rare regions of low expression, usually a small cluster of cells. n. Detecting difference of expression level is difficult at this age, since there are very rare regions of no expression. Many cells that express Vamp1 at high levels display the flame shape (dashed lines) but not all. p. Vamp1 expression next to the infundibulum is moderate in the basal layer and includes a layer in the granular layer as well, seen as a line above the basal layer.

q-s Vamp1 and K10: q, u. Vamp1 and K10 expression do not colocalize. K10 is a marker of differentiation and usually found in suprabasal layers of the epidermis. Vamp1 is found in the basal layer, where undifferentiated stem cells are found. Where Vamp1 is expressed the strongest, K10 is expressed stronger in the cells above it.

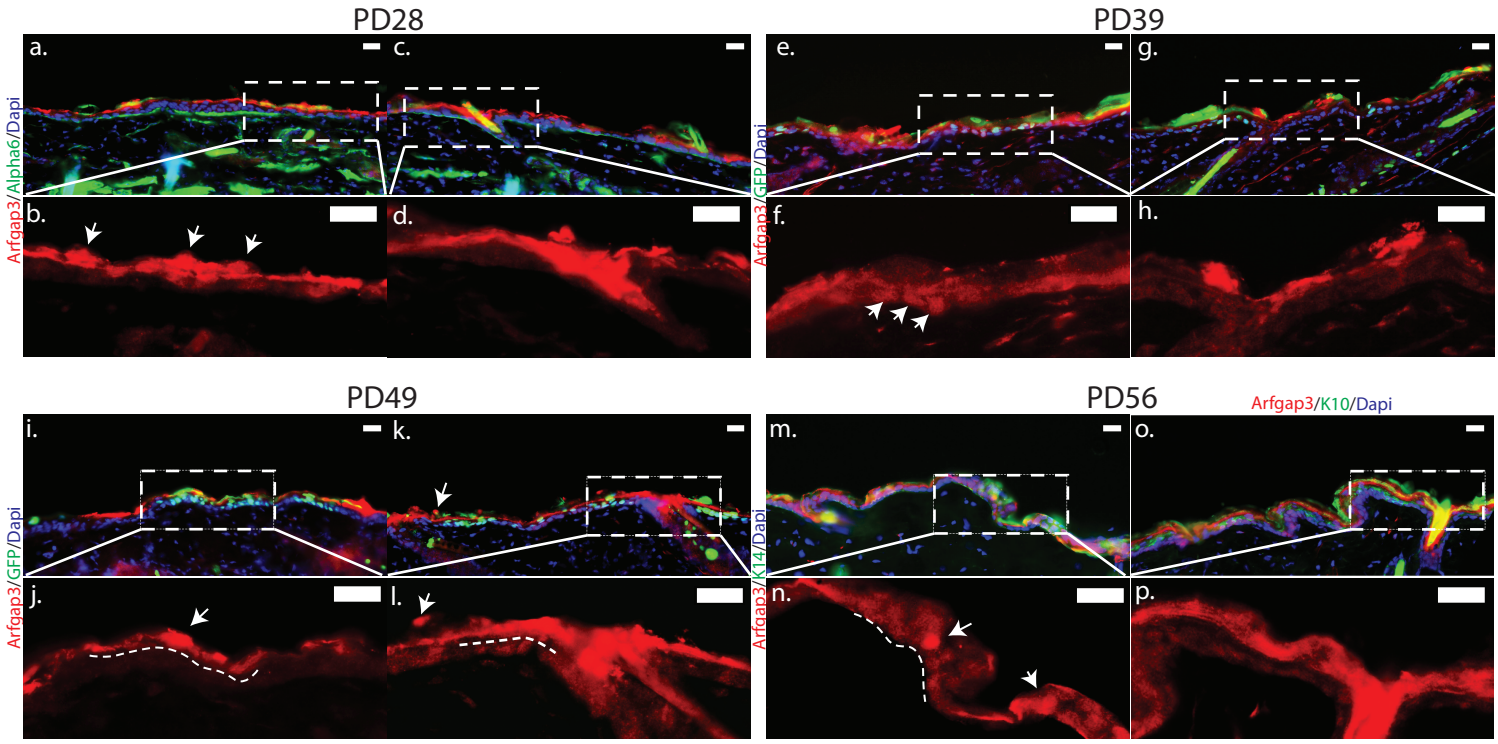

Figure 4 Arfgap3 expression in mouse back skin at varying time points.

a-d PD28: a. Arfgap3 is expressed primarily in the granular layer as a heterogenous line. b. Rare cells expressing Arfgap3 at a higher level are seen in what could be either the upper granular layer or cornified layer (arrows). c, d. Expression increases near the infundibulum, and more consistent domain expression is observed.

e-h PD39: e. Expression is now seen in the basal and the spinous layer but generally as background. f. Individual cells can be detected with higher expression but not always at a significant difference from the background (arrows). g, h. Domains of highly expressing cells can be seen at the infundibulum. The line of expression seen previously in the granular layer is no longer as strong nor homogenous.

i-l PD49: i. Background expression is found in granular, spinous, and basal layers. j. Rare cells expressing higher levels are found in all these layers (arrows). Heterogeneity between granular layer expression in IFE vs infundibulum continues (dashed lines).

m-p PD56: m, o. The homogenous granular expression can be seen again. n. Background expression is higher in many cells (dashed line), with rare cells of higher expression (arrows). o, p. Expression is higher at infundibulum, and individual cells are more difficult to identify.

Examination of Vamp1-stained skin sections showed broad expression in the basal layer at all the time points analyzed (Fig 3). These domains varied at the different time points observed. Vamp1 expression in cells of the epidermis appears to consistently be in the plasma membrane and cytosol, with clear nuclear voids observed in single color channel imaging (Fig 3) as expected for this protein (see Table 1). The Vamp1 expression in the epidermal basal layer was somewhat variable, suggestive of potential heterogeneity. At the earliest observed timepoint (PD28) Vamp1 expression displayed the greatest heterogeneity, with small domains of three to five highly expressing cells clustered in the basal layer flanked by short stretches of epidermis with lower expression (Fig 3a). Intriguingly, basal layer cells with less expression show Vamp1 polarized at the basal membrane contacting side (Fig 3b) whereas the highly expressing basal cells show Vamp1 more polarized at the apical side (Fig 3n, t). Near the infundibulum, there tends to be a larger, consistently high expressing group of cells in the basal layer of the epidermis (Fig 3c). This group of cells is linear or non-interrupted by low expressing epidermal basal cells and continues down into the outer root sheath of the infundibulum into the hair follicle (Fig 3d). This was interesting since the LRC domains in the tail skin are known contain the hair follicles.

Across all these timepoints, I noticed frequently, that cells which express Vamp1 more are shaped differently from other basal layer cells. Most of the basal layer cells expressing Vamp1 at low or background levels are flattened to varying degrees (Fig 3j, l). The cells that express Vamp1 at higher levels often have a flame shape, with the basal membrane side wide and the side next to the spinous layer forming a point (Fig 3b, f, n). While this is not true of all cells expressing Vamp1 at higher levels, it is a common observation.

Arfgap3 stained skin sections also showed heterogenous expression and presented some variations at the time points analyzed. Epidermal cells express Arfgap3 throughout the cell body including the nucleus (Fig 4). The earliest observed time point (PD28) displayed Arfgap3 expression in what appear to be the granular or cornified layer (Fig 4a-d) pending co-localization with granular layer markers such as involucrin and loricrin. Some of these cells appear flattened while others retain round shapes, and many were negative for DAPI (were anuclear) suggesting they were part of the cornified envelope. Arfgap3 expression was observed to be highly heterogenous in the basal and spinous layers. Some domains were made of groups of high expressing cells while in other places there were singular cells. Background expression in the granular/cornified layer is generally higher than in the basal and spinous layers and is more consistent throughout the stages. Near the infundibulum Arfgap3 expression becomes more homogenous throughout the epidermal layer with individual cells difficult to identify (Fig 4d, h, l, p). Over the subsequent observed timepoints (PD39, 49, 56) expression expanded to the basal layer (Fig 4f, i, I, n, p). By PD56, rare individual cells express Arfgap3 more while the epidermis continues to show a low level of background expression (Fig 4n), though more than at the initial timepoint of PD28.

In summary, Vamp1 and Arfgap3 are both expressed in the epidermis. Vamp1 is mostly a basal layer marker, with some gaps in expression within the basal layer at PD28, that are less prominent at later time points. In contrast, Arfgap3 is mostly found in the granular layer or cornified envelope with some expression in rare basal cells or clusters of basal cells at the later stages. Intriguingly, both proteins showed increased expression in the vicinity of the hair follicle infundibulum.

B2. Complex patterns of Vamp1 and Arfgap3 colocalization with LRCs in mouse back skin.

In order to understand where Vamp1 and Arfgap3 are expressed in relation to epidermal LRCs, I stained skin isolated from K5-tTA x pTRE-H2BGFP mice (Sada A et al, 2016) H2B-GFP subjected to two-week doxycycline chase. Interestingly, I found that neither Vamp1 nor Arfgap3 are expressed in the brightest LRCs indicative of the fewest divisions. LRCs that have divided already and show a reduced label signal are more likely to contain IF signal for these gene products. In mouse back skin, Vamp1 most regularly shows the greatest degree of colocation with some LRCs near the infundibulum (Fig 5a). The Vamp1 domain is often found next to the bright clustering LRCs, overlapping the midrange LRCs and expanding into cells without label nearby (Fig 5b, c). Arfgap3 domains in the granular layer overlap with LRC granular expression with some offset (Fig 5g). Individual cells that highly express Arfgap3 are more likely to be midrange LRCs (Fig 5h, i), but not all midrange LRCs express Arfgap3 more than the surrounding background (Fig 5k, l).

Despite our expectation of Vamp1 and Arfgap3 to specifically be expressed in the brightest LRCs, our in-situ analysis suggests that expression may be more prominent in the midrange LRCs and absent in the brightest LRCs. This suggests additional heterogeneity in the LRC lineage, which was masked in the microarray data based on a mixed population of bright and mid-range LRCs. Further data and quantification will be required to confirm these experiments and fully define the expression of these markers relative to LRC populations in the epidermis. Single cell RNAseq data of the epidermal LRCs may provide further insight into the heterogeneity of gene expression in this lineage.

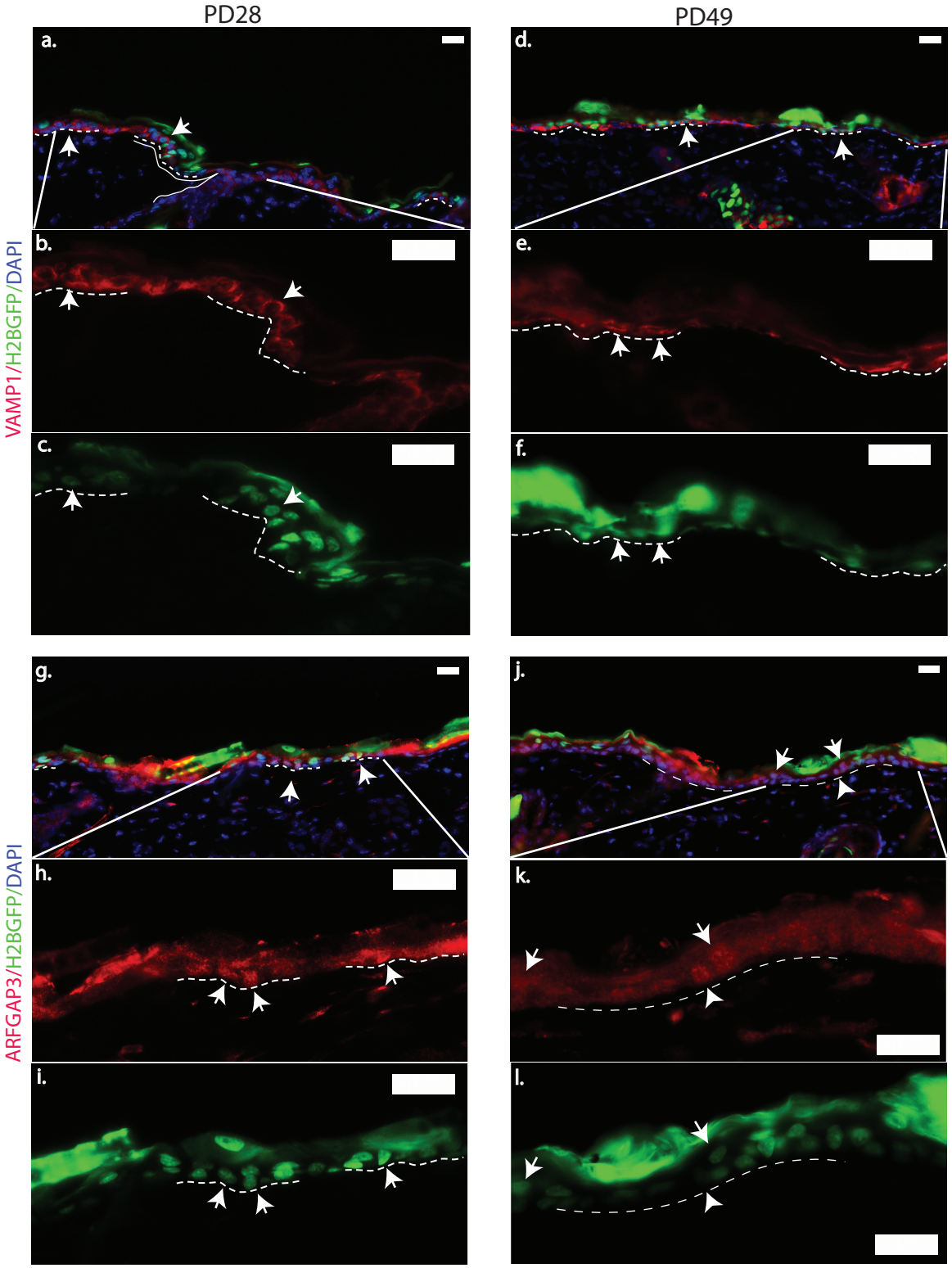

Figure 5 Vamp1 and Arfgap3 expression compared to LRC location.

a-c PD28 Vamp1 and H2BGFP expression: a. Vamp1 expression is does not collocate with the LRCs retaining the most label but is expressed higher next to groups of LRCs. Areas of overlap marked with dashed line. Infundibulum marked with solid line. Within the high expressing Vamp1 areas, are some LRCs but not necessarily the same cells. Cells that expresss both Vamp1 and H2B-GFP distinguishably are rare (arrows). b, c. Where Vamp1 expression is higher, only rare cells if any retain the H2BGFP label. Colocalization marked with arrows.

d-f PD49 Vamp1 and H2BGFP expression: a. Vamp1 is expressed in heterogenous domains that overlaps with LRC domains, though not comepletely. b, c. Vamp1 expression collocates with cells that retain some but not all of the H2BGFP label (arrows).

g-i PD28 Arfgap3 and H2BGFP expression: g. Arfgap3 expression does not collocate with the LRCs retaining the most label. h, i. It is expressed by cells retaining some of the H2BGFP label (arrows).

j-l PD49 Arfgap3 and H2BGFP expression: j. Arfgap3 expression still collocates with cells weakly retaining the H2BGFP label, but these cells express Arfgap3 only slightly more than the background. k, l. The cells expressing Argfgap3 the most are not LRCs (arrowheads).

B3. Expression of Vamp1 in human skin.

Given the heterogenous expression of Vamp1 and Arfgap3 expression in mouse skin, I wanted to see if the pattern held in human skin as well. Human skin structure is different from that of mice; the basal membrane between epidermis and dermis undulates creating rete ridges and dermal papillae (Fig 6i). Rete ridges are distal to the skin surface while dermal papillae are proximal. Previous work has described these structures using epidermal and proliferative markers and lead to the conclusion stem cells are located at the dermal papillae (Lawlor KT, Kaur P, 2015). Based on previous studies of proliferation in human basal layer we hypothesized that LRCs may be found at the dermal papillae and non-LRCs may be near the rete ridges.

The two human samples I first analyzed, were both from aged individuals (over the age of 65) and both genes of interest, Vamp1 and Arfgap3, were co-stained with K10. Reminiscent of the results in mouse back skin, Arfgap3 was expressed strongly in the granular layer and was indistinct near the dermal papillae and rete ridges, appearing weak if present at all throughout the basal layer. Moving upwards from the spinous to granular layers, it started to show expression in the nucleus, and was expressed strongly in the granular layer showing an intense band of fluorescence (Fig 6 a-d). Thus, Arfgap3 did not display a pattern of heterogeneity between the rete ridges and dermal papillae. This may due to the advanced age of the donor samples, and further investigation in younger donors may provide more insight into the expression of Arfgap3 in human skin.

Vamp1 expression was also reminiscent of mouse back skin, with strong expression in the basal layer. The skin sample had flattened out somewhat

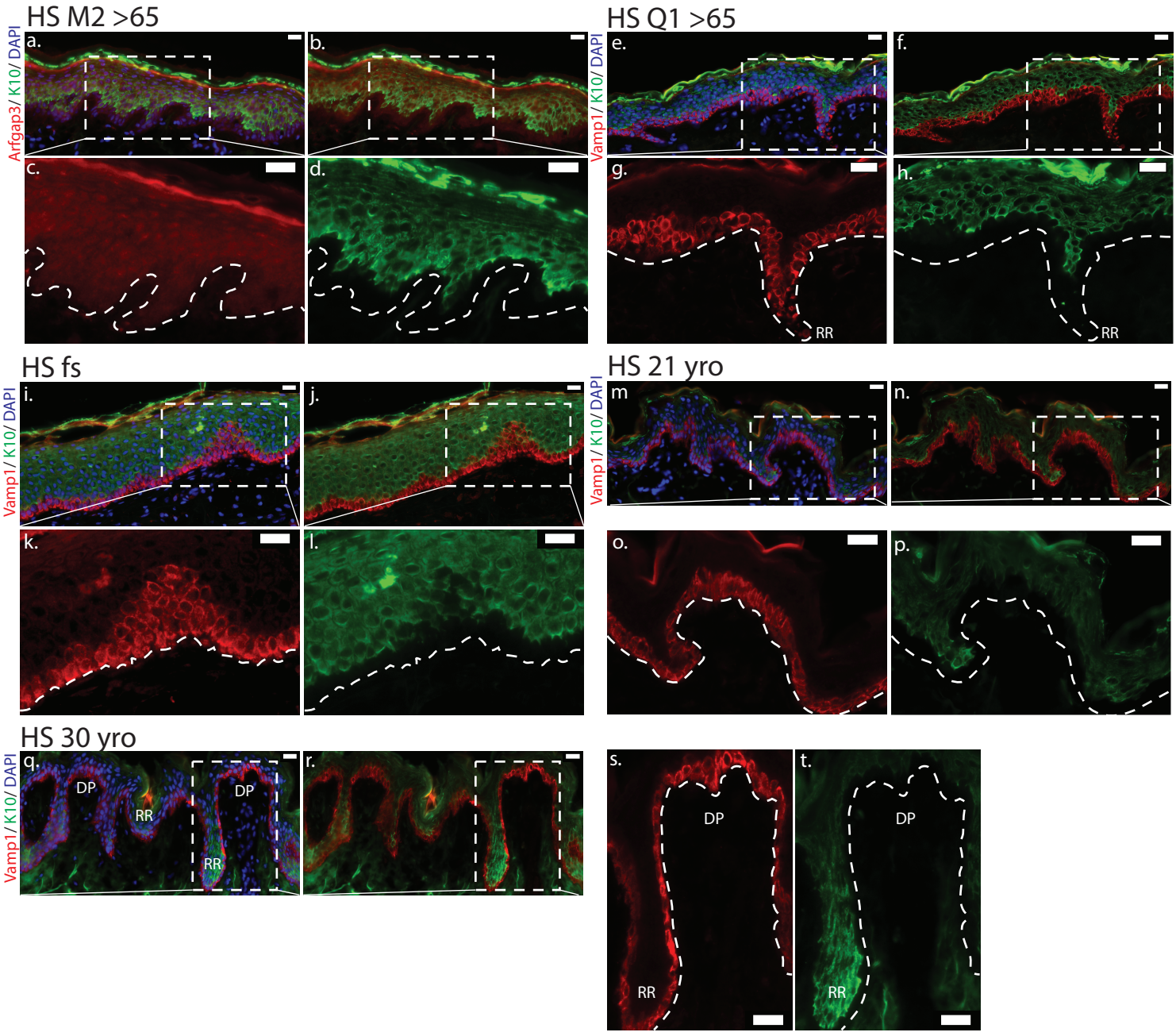

Figure 6 Vamp1 and Arfgap3 expression in human skin. Dashed lines indicate basal layer.
a-d HS M2 >65 yro Arfgap3 and Keratin 10: a, b. As seen in mouse skin, Arfgap3 is expressed strongly in the cornified layer as a continuous line. c. It is expressed in the granular and spinous layer, but expression is considerably less in the basal layer. There is no overlap of increased Arfgap3 expression with potential LRC location.
e-h HS Q1 >65 yro Vamp1 and Keratin 10: e,f. Vamp1 is seen throughout the basal layer in domains of high and low expression, similar to expression in mouse skin. Dermal papillae are rare, likely due to age of sample.
i-l HS foreskin Vamp1 and Keratin 10: i. Vamp1 is expressed throughout the basal layer. The epidermis has not developed the distinctive folds of dermal papillae and rete ridges yet. k. Vamp1 is expressed above the basal layer in regions likely to develop into dermal papillae.
m-p 20 yro Vamp1 and Keratin 10: . Vamp1 is strongly expressed in the basal layer.
q-t HS 30 yro Vamp1 and Keratin 10: q, s. Expression is level is higher in the dermal papillae (DP), and lower in the rete ridges (RR). t. Keratin 10, a marker of differentiation, is expressed in the rete ridges.

though, and the dermal papillae and rete ridges were not distinct. I stained human samples at ages <1 month, 21 years, 30 years, with Vamp1 and K10 antibodies (Figure 6e-p). As with mouse skin, Vamp 1 was strongly and exclusively present in the basal layer of the epidermis and was not expressed in the supra-basal layers. There may be some evidence from my data of increased expression in the dermal papillae relative to rete ridges, but this requires further investigation (see for example Figure 6k). In fact, a follow-up experiment by Joydeep Baidya and Sangeeta Ghuwalewala in our laboratory, suing higher dilution of the Vamp1 antibody revealed better differences in expression between the dermal papillae and the rete ridges (data not shown).

Finally, I observed that basal layer cells located at the dermal papillae that expressed Vamp1 more had morphology similar to that seen in highly expressing Vamp1 cells in mouse skin (Fig 6f, g, i, j). This flame-shape morphology does not appear to be quite as consistent though and requires further study and quantification. It may be that higher levels of Vamp1 in epidermal basal cells dictate this morphology, but the functional significance of this remains to be unraveled by future knockout studies.

CHAPTER 3

Discussion

Based on the results from the microarray mining, I expected to observe clearly expressed genes in heterogenous patterns colocalizing with epidermal LRCs. The five LRC marker candidates analyzed with IF staining seemed ideal based on normalized gene expression, however only two of the five candidates, namely Arfgap3 and Vamp1, displayed a discernable signal and brought some preliminary evidence towards the hypothetical heterogeneity. Although not all epidermal basal layer cells expressed equal levels of Arfgap3 and Vamp1, their expression in our hypothesized domains is broader and less distinct that we had hoped for initially. Furthermore, the expectation of colocalizing with LRCs was also unmet. I expected to see Vamp1 and Arfgap3 clearly and preferentially expressed by cells that most retained the H2B-GFP label. I expected if Vamp1 or Arfgap3 was seen in other cells, it would be at a lower level and easily discernable to the eye. I also expected this pattern to be the same throughout adult skin homeostasis. None of these expectations were met, but the preliminary data revealed something unexpected and interesting.

Vamp1 and Arfgap3 seem to be expressed more in some cells that retain medium H2B-GFP label but not in the brightest cells. This indicates epidermal stem cells are not binary LRCs or non-LRCs; that LRCs are likely further split into brightest LRCs and medium LRCs. These midrange LRCs could be a separate group of stem cells by themselves or they might be progenitor cells derived from the brighter LRCs.

These Vamp1 and Arfgap3 domains also appear temporally dynamic, changing with age and potentially the hair cycle. It is known that epidermal basal layer cells proliferate more during anagen, and I observed more expression of

both Vamp1 and Arfgap3 in the epidermal basal layer during this stage. At this time, there are not sufficient data to support either age or hair cycle as the driving factor for the dynamic heterogeneity observed. We can only say the expression changes over time. Expression varies within the domains as well, with preferential expression polarized within cells or in sub populations.

My studies were conducted in uninjured mouse back skin, which displays scale and interscale regions (Sada A et al, 2016) but is not well defined. Mouse tail skin has a much more defined scale and interscale structure (Sada A et al, 2016). Future studies should include defining Vamp1 and Arfgap3 expression in mouse tail skin and how dynamic this expression is over time as well. The initial studies in human skin are promising as well, with sufficient promise for further studies. Continuing this line of research future studies could sort LRCs by intensity of fluorescent label to create a gradient of LRCs, and then analyze for Vamp1 and Arfgap3 expression in each group using the primers and conditions I have tested here to quantitatively compare the expression of these markers in LRCs and non-LRCs and confirm the microarray results. I would study the expression of these two genes in developing skin, at varying time points between PD1 and PD21, using whole skin and sorted cells in qRT-PCR, and whole skin samples in IF analysis. Use of conditional knock-out mouse lines to study Vamp1 and Arfgap3 could help identify their importance in skin maintenance and healing as well and perhaps provide an answer for the biological role of heterogeneous domains of gene expression in the epidermis. I would also attempt to raise mice to at least 12 months to observe expression in aged skin homeostasis and wound repair (Nishiguchi M et al., 2018).

Both Vamp1 and Arfgap3 are involved in vesicle transport and targeting but have different effects on cell function. Mutations in Vamp1 lead to spastic

ataxia (VAMP1, 2019) and transgenic knock-out lines do not survive weaning due to a lethal wasting phenotype (004626 - C3H/HeSnJ-*Vamp1*^{lew}/GrsrJ, 2019). Afgap3 is a member of the Ras superfamily of small GTP-ases, which are associated with cell proliferation, differentiation and survival and have been linked to cancer, though most often through upstream mutations (Cromm PM et al, 2015). Interestingly, extracellular vesicles have been identified as a key method of cell-to-cell communication in both stem and cancer cells (French KC et al., 2017). This could explain why the microarray indicated both these genes were upregulated in the basal and spinous layer LRCs. There is also the pattern of the neural epithelial junction; nerves approach the epidermis at discrete locations. There could be coordination or communication between the nerve filaments and LRCs, made possible by Vamp1 expression which is a key component of synaptic vesicle docking (VAMP1, 2019).

CHAPTER 4

Methods

A. RNA isolation and qRT–PCR.

Total RNAs were isolated from whole skin and sorted skin cells prepared by using RNeasy (Qiagen) and used for reverse transcription by Super script III (Invitrogen). Primers were designed for each gene of interest (Table 2). Published literature was searched but did not yield results compatible with goals. The Primer3 website (http://bioinfo.ut.ee/primer3/) was used to design all primers. Primers were designed to amplify regions 150 to 250 base pairs in length, with ideal length around 150 base pairs. The primers were also designed to align to all known isoforms of each gene and according to Pubmed Primer Blast. The primers used were as follows: Gapdh, 5'-ACTGCCACCCAGAAGACTGT-3' and 5'-GATGCAGGGATGATGTTCT-3'; Vamp1, 5'-AGAGTTCCGGGTGTTTCGTG-3' and 3'-CCGCCTGTTACTGGTCATGT-5'; Nagk, 5'-GCACAAACCACTGGCTGATT-3' and 3'-CGGTGCCTCAACTCCTCAAT-5'; LIF, 5'-GGCAACCTCATGAACCAGATC-3' and 3'-TCTGGTCCCGGGTGATATTG-5'; Cacul1, 5'-AACACCTCCACCTCCAAGTT-3' and 3'-CTGCTGGCACACACACTTAT-5'; Arfgap3, 5'-TCTAGCTGGGATGATGGTGC-3' and 3'-TGAAGAGATGGCCTTGACGT-5'; Etfdh, 5'-TGAGCTGGATGGGAGAACAG-3' and 3'-ACTTTGGCATGCAGTTCCAG-5';Arhgef28, 5'-AGTCTTGGAGTCTCGTGGTG-3' and 3'-AGCTGCAGTTCCTCCTTCAT-5'.

B. Mice.

All mouse experiments were carried out according to Cornell University Institutional Animal Care and Use Committee guidelines (protocol number no. 2007-0125). Samples from K5-tTA x pTRE-H2BGFP mice (Sada A et al, 2016) were provided courtesy of Sangeeta Ghulewalewala, who conducted doxycycline chase, harvested tissue, and embedded in OCT medium. Mice were fed with

doxy chow (1 g doxy/1 kg, Bio-serv) for the indicated chase periods, starting at 1–3 months of age. All other samples were collected from wild-type mice. The sample size was dictated by availability of mice and need for quality samples. Statistical needs were not accounted for. Both male and female mice were used for all experiments. These experiments were not blinded.

C. Immunostaining of skin sections.

Mouse back skin was collected and embedded in Optimal Cutting Temperature (OCT) compound (Tissue Tek, Sakura). Human skin samples arrived embedded in OCT from collaborators. Samples were cut frozen 10μm thick and were fixed in 4% PFA for 10 min at room temperature. After blocking in normal serum for two hours, sections were incubated with primary antibodies for one hour at room temperature. Sections were then washed and incubated with secondary antibodies for one hour at room temperature. Sections were washed again and counterstained with Hoeschst then mounted.

Primary antibody dilutions: rabbit anti-Arfgap3 (1:500, Proteintech no. 15293-1-AP), rabbit anti-Vamp1 (1:500, Proteintech no. 13115-1-AP 1:500), mouse anti-K14 (1:300, Abcam no. ab7800), mouse anti-K10 (1:1000, Abcam no. ab9026), rat anti-CD49f (α6-integrin) (1:200, BD Pharmingen no. 555734). Rabbit anti-Nagk (Proteintech no. 15051-1-AP), rabbit anti-Rpap2 (Proteintech no. 17401010AP) and rabbit anti-Ragpgef4 (Proteintech no. 19103-1-AP) were tested at varying dilutions without clear resolution (Table 3). All secondary antibodies (TxR, FITC, or Alexa-594, Jackson ImmunoResearch) were used at a 1:500 dilution. The MOM kit (Vector Laboratories) was used for blocking with primary antibodies as needed.

D. Microscope images.

Skin samples were examined using a fluorescent microscope (Nikon) and digitally imaged using a CCD (charge-coupled device) 12-bit digital camera (Retiga EXi; QImaging) and IP-Lab software (MVI). Images were enhanced in Adobe Photoshop by manipulating brightness and contrast only.

E. Rigor and reproducibility.

The qRT-PCR analysis was conducted with samples obtained from two different mice in both whole skin and sorted cell analysis. As the immunofluorescent experiments are preliminary, they were conducted with samples from one mouse at each age reported, though samples were collected from different regions of the back. The experiments on human skin were also conducted with one sample per age reported. They must be repeated in a minimum of 3 mice per time point and followed up with quantification of images using Image J and statistical analysis using JUMP and the t t-test to compare the level of expression Vamp1 in LRCs and non-LRCs. For immunostaining multiple experiments were performed as follows: ten experiments on wild type mice samples testing various dilutions of potential LRC markers and co-staining with various epidermal markers were conducted in PD49 and PD56 skin to determine best resolution of heterogenous expression; four experiments on K5-tTA x pTRE-H2BGFP mice samples to identify potential LRC marker colocalization with LRCs; four experiments on wild type mice using potential LRC markers and epidermal markers; two experiments on human samples using potential LRC markers and epidermal markers.

REFERENCES

Sada A, et al. Defining the cellular lineage hierarchy in the interfollicular epidermis of adult skin. *Nat Cell Biol*. 2016;18(6):619-31.

ARFGAP3 ADP ribosylation factor GTPase activating protein 3 [*Homo sapiens* (human)]. (updated 2019, February 13). Retrieved from https://www.ncbi.nlm.nih.gov/gene/26286

ARFGAP3 localizations. (accessed 2019, March). https://compartments.jensenlab.org/Entity?figures=subcell_cell_%%&knowledge=10&textmining=10&predictions=10&type1=9606&type2=-22&id1=ENSP00000263245

VAMP1 vesicle associated membrane protein 1 [*Homo sapiens* (human)]. (updated 2019, February 26). Retrieved from https://www.ncbi.nlm.nih.gov/gene/6843

Salpietro V, et al. Homozygous mutations in VAMP1 cause a presynaptic congenital myasthenic syndrome. *Ann Neurol*. 2017;81(4):597–603.

VAMP1 localizations. (accessed 2019, March). Retrieved from https://compartments.jensenlab.org/Entity?figures=subcell_cell_%%&knowledge=10&textmining=10&predictions=10&type1=9606&type2=-22&id1=ENSP00000379602

Kubo Y, et al. ABCA5 resides in lysosomes, and ABCA5 knockout mice develop lysosomal disease-like symptoms. *Mol Cell Biol*. 2005;25(10):4138-49.

DeStefano GM, et al. Mutations in the cholesterol transporter gene ABCA5 are associated with excessive hair overgrowth. *PLoS Genetics*. 2014;10(5):e1004333.

Hayashi R, et al. First Japanese case of congenital generalized hypertrichosis with a copy number variation on chromosome 17q24. Journal of Dermatological Science. 2017;85(1): 63-65.

Dembla M, et al. ArfGAP3 Is a Component of the Photoreceptor Synaptic Ribbon Complex and Forms an NAD(H)-Regulated, Redox-Sensitive Complex with RIBEYE That Is Important for Endocytosis. *Journal of Neuroscience*. 2014;34(15):5245-5260.

Tšuiko O, et al. Copy number variation analysis detects novel candidate genes involved in follicular growth and oocyte maturation in a cohort of premature ovarian failure cases. *Hum Reprod*. 2016;31(8):1913-25.

Miller NL, et al. Rgnef (p190RhoGEF) knockout inhibits RhoA activity, focal adhesion establishment, and cell motility downstream of integrins. *PLoS One*. 2012;7(5):e37830.

Miller NL, et al. A non-canonical role for Rgnef in promoting integrin-stimulated focal adhesion kinase activation. *J Cell Sci*. 2013;126(Pt 21):5074-85.

Nakahara H, et al. Activation of β1 Integrin Signaling Stimulates Tyrosine Phosphorylation of p190*RhoGAP* and Membrane-protrusive Activities at Invadopodia. *The Journal of Biological Chemistry.* 1998;273(1):9-12.

Lim Y, et al. PyK2 and FAK connections to p190Rho guanine nucleotide exchange factor regulate RhoA activity, focal adhesion formation, and cell motility. *J Cell Biol*. 2008;180(1):187-203.

Lim ST, et al. Knock-in mutation reveals an essential role for focal adhesion kinase activity in blood vessel morphogenesis and cell motility-polarity but not cell proliferation. *J Biol Chem*. 2010;285(28):21526-36.

Kigoshi Y, et al. CACUL1/CAC1 Regulates the Antioxidant Response by Stabilizing Nrf2. *Scientific Reports*. 2015;5:e12857.

Xu J, et al. *ETFDH* Mutations and Flavin Adenine Dinucleotide Homeostasis Disturbance Are Essential for Developing Riboflavin-Responsive Multiple Acyl–Coenzyme A Dehydrogenation Deficiency. Annals of Neurology. 2018;84(5):659-673.

Roselló-Lletí E, et al. Heart mitochondrial proteome study elucidates changes in cardiac energy metabolism and antioxidant PRDX3 in human dilated cardiomyopathy. *PLoS One*. 2014;9(11):e112971.

Sharif SR, Islam A, Moon IS. N-Acetyl-D-Glucosamine Kinase Interacts with Dynein-Lis1-NudE1 Complex and Regulates Cell Division. *Mol Cells*. 2016;39(9):669-79.

Seo H, Lee K. Epac2 contributes to PACAP-induced astrocytic differentiation through calcium ion influx in neural precursor cells. *BMB Rep*. 2016;49(2):128-33.

Pereira L, et al. Epac2 mediates cardiac β1-adrenergic-dependent sarcoplasmic reticulum Ca2+ leak and arrhythmia. *Circulation*. 2013;127(8):913-22.

Zhang CL, et al. The cAMP Sensor Epac2 Is a Direct Target of Antidiabetic Sulfonylurea Drugs. *Science*. 2009;325(5940):607-610.

Wallner M, et al. Exenatide exerts a PKA-dependent positive inotropic effect in human atrial myocardium: GLP-1R mediated effects in human myocardium. *Journal of Molecular and Cellular Cardiology*. 2015;89(B):365-375.

Masyuk AI, et al. Cholangiocyte primary cilia are chemosensory organelles that detect biliary nucleotides via P2Y12 purinergic receptors. *American Journal of Physiolology Gastrointestal Liver Physiology*. 2008;295(4):G725-34.

Guglielmi V, et al. Abnormal expression of RNA polymerase II-associated proteins in muscle of patients with myofibrillar myopathies. *Histopathology.* 2015;67:859–865.

Forget D, et al. Nuclear import of RNA polymerase II is coupled with nucleocytoplasmic shuttling of the RNA polymerase II-associated protein 2. *Nucleic Acids Res*. 2013;41(14):6881-91.

Corderiro JM, et al. Synaptotagmin 1 is required for vesicular Ca^{2+}/H^{+}-antiport activity. *Journal of Neurochemistry*. 2013;126(1):37-46.

Morgenthaler FD, et al. Morphological and molecular heterogeneity in release sites of single neurons. *European Journal of Neuroscience*. 2003;17(7):1365-1374.

Nystuen AM, et al.
A null mutation in VAMP1/synaptobrevin is associated with neurological defects an d prewean mortality in the lethal-wasting mouse mutant.
Neurogenetics. 2007;8(1):1-10.

Peng L, Adler M, Demogines A, et al. Widespread sequence variations in VAMP1 across vertebrates suggest a potential selective pressure from botulinum neurotoxins. *PLoS Pathog*. 2014;10(7):e1004177.

Riffault B, et al. Pro-Brain-Derived Neurotrophic Factor Inhibits GABAergic Neurotransmission by Activating Endocytosis and Repression of $GABA_A$Receptors. *Journal of Neuroscience.* 2014;34(40):13516-13534.

Tsai PS, et al. Preparation of the Cortical Reaction: Maturation-Dependent Migration of SNARE Proteins, Clathrin, and Complexin to the Porcine Oocyte's Surface Blocks Membrane Traffic until Fertilization. *Biology of Reproduction*. 2011;84(2):327–335.

Rossetto O, et al. VAMP/synaptobrevin isoforms 1 and 2 are widely and differentially expressed in nonneuronal tissues. *The Journal of Cell Biology*. 1996;132(1);167-179.

Duregotti E, et al. Snake and Spider Toxins Induce a Rapid Recovery of Function of Botulinum Neurotoxin Paralysed Neuromuscular Junction. *Toxins.* 2015;*7*(12):5322-5336.

Lawlor KT, Kaur P. Dermal Contributions to Human Interfollicular Epidermal Architecture and Self-Renewal. *Int J Mol Sci*. 2015;16(12):28098-107.

Nishiguchi M et al., Aging Suppresses Skin-Derived Circulating SDF1 to Promote Full-Thickness Tissue Regeneration. *Cell Reports*. 2018; 24:3383–3392.

004626 - C3H/HeSnJ-*Vamp1*^{lew}/GrsrJ. (Updated 2019). Retrieved from https://www.jax.org/strain/004626

Cromm PM et al., Direct Modulation of Small GTPase Activity and Function. *Angewandte Chemie. Int. Ed*. 2015; 54: 13516-13537.

French KC et al., Extracellular vesicle docking at the cellular port: Extracellular vesicle binding and uptake. *Semin Cell Dev Biol*. 2017;67:48-5